



Contribution of the Hall term in small-scale magnetohydrodynamic dynamosArijit Halder ¹, Supratik Banerjee ^{1,*}, Anando G. Chatterjee,² and Manohar K. Sharma¹¹*Department of Physics, Indian Institute of Technology, Kanpur 208016, India*²*Computer Centre, Indian Institute of Technology, Kanpur 208016, India*

(Received 7 March 2023; accepted 20 April 2023; published 4 May 2023)

A detailed study of small-scale Hall magnetohydrodynamic dynamos has been performed both analytically and numerically. Assuming the magnetic field and the current to be separate fields, the contribution of the Hall term has been decomposed into two parts and their individual contributions have been studied separately. Calculating the scale-separated transfer rates described in Dar *et al.* [*Physica D* **157**, 207 (2001)], it is found that the small-scale current fields are the primary contributors in sustaining large-scale magnetic fields. Furthermore, the nature of the scale-to-scale fluxes are found to be globally intact with the ion inertial scale.

DOI: [10.1103/PhysRevFluids.8.053701](https://doi.org/10.1103/PhysRevFluids.8.053701)**I. INTRODUCTION**

A turbulent flow is characterized by its prevalent nonlinearity over viscous properties [1]. For the Navier-Stokes equations, this nonlinearity is represented by the velocity advection term $(\mathbf{u} \cdot \nabla)\mathbf{u}$, where \mathbf{u} is the fluid velocity [2,3]. For a magnetohydrodynamic (MHD) fluid, the nonlinearity in the momentum equation is represented by both $(\mathbf{u} \cdot \nabla)\mathbf{u}$ and the Lorentz force term $\mathbf{J} \times \mathbf{B}$, where \mathbf{B} is the magnetic field and $\mathbf{J} = \mu_0^{-1}(\nabla \times \mathbf{B})$ is the current density [4,5]. In the case of ordinary MHD turbulence, the induction equation takes the form

$$\frac{\partial \mathbf{B}}{\partial t} = \nabla \times (\mathbf{u} \times \mathbf{B}) + \eta \nabla^2 \mathbf{B}, \quad (1)$$

where the first term on the right-hand side represents the nonlinear contribution and the second term represents the diffusion, η being the magnetic diffusivity. Similar to hydrodynamic turbulence, in MHD we also observe cascade of total energy (kinetic + magnetic), which is an inviscid invariant of the system. It is important to note that, in the ordinary MHD model, ions and electrons move with the same velocity (the fluid velocity) [5,6]. However, this does not remain valid for length scales close or smaller to the ion inertial length d_i . For those length scales, it is important to include the effect of finite difference between the ion and electron velocities [7]. This effect is incorporated in the induction equation by adding a nonlinear term $-\nabla \times (\mathbf{J} \times \mathbf{B})/ne$, often called the Hall term, where n and e are the number density of the electrons or ions and the electronic charge, respectively, and the corresponding model is known as Hall MHD (HMHD). In terms of $\mathbf{b} (= \mathbf{B}/\sqrt{\mu_0\rho})$, with ρ being the mass density of the MHD fluid), the magnetic field normalized to a velocity and $\mathbf{j} = \nabla \times \mathbf{b}$, the induction equation simply gives the evolution of \mathbf{b} and the corresponding Hall term can be written as $-d_i \nabla \times (\mathbf{j} \times \mathbf{b})$. Despite having different ion and electron velocities, HMHD is a monofluid model and cannot capture all the essential aspects of sub-ion-scale plasma dynamics including the kinetic effects. However, HMHD turbulence is often found quite useful to probe into the sub-ion-scale turbulence in the space and astrophysical plasmas [8,9].

*sbanerjee@iitk.ac.in

Several aspects of HMHD turbulence (both incompressible and compressible) have been explored analytically, numerically, and also using *in situ* spacecraft data during the last two decades. Besides systematic studies covering the basic features like energy cascade, power-spectrum, universal scaling, dissipative anomaly, etc. [10–15], some interesting studies have also been made exploring the importance of HMHD turbulence in the heating of the solar wind and other space plasmas [16–19]. A dynamo mechanism is essential to explain long-lasting magnetic fields in astrophysical plasmas [20–22]. Whereas a sustained large-scale magnetic field can be explained in terms of mean-field MHD and HMHD, a turbulent dynamo mechanism is often useful to explain the development and energization of magnetic field fluctuations of length scales inferior to the external forcing scale (small-scale dynamo) [23–28]. Unlike ordinary MHD, where the dynamo action can be explained in terms of the advection and deformation of the magnetic field tubes in the bulk fluid, the dynamo action in HMHD can be explained using the generalized velocity-vorticity formulation proposed in Ref. [29]. The induction equation in ideal HMHD can be written as $\partial_t \mathbf{b} = \nabla \times (\mathbf{u}_e \times \mathbf{b}) = -(\mathbf{u}_e \cdot \nabla) \mathbf{b} + (\mathbf{b} \cdot \nabla) \mathbf{u}_e$, where $\mathbf{u}_e = \mathbf{u} - d_i \mathbf{j}$ is the electron fluid velocity. HMHD dynamos can thus be thought to be caused by the motion and the deformation (stretching) of magnetic tubes in electron fluid. Equivalently, combining the vorticity and the induction equation, for generalized vorticity $\mathbf{\Omega} (= \mathbf{b} + d_i \boldsymbol{\omega})$, one obtains $\partial_t \mathbf{\Omega} = \nabla \times (\mathbf{u} \times \mathbf{\Omega}) = -(\mathbf{u} \cdot \nabla) \mathbf{\Omega} + (\mathbf{\Omega} \cdot \nabla) \mathbf{u}$, where $\boldsymbol{\omega} = \nabla \times \mathbf{u}$. As a result, HMHD dynamos can also be regarded as the advection and deformation of generalized vorticity tubes in the ion fluid (as the ion velocity \mathbf{u}_i is approximately equal to the bulk velocity \mathbf{u}). The role of Hall effect in small-scale dynamos has been studied using numerical simulations both for helical and nonhelical forcings [26,30]. Using a resolution of 256^3 , both studies reported a backscatter (to larger scales) of magnetic energy due to the Hall term. The flux rates due to the Hall term were found to be approximately 10–15 times weaker than the MHD flux rates. The Hall contribution was calculated from the entire $-d_i \nabla \times (\mathbf{j} \times \mathbf{b})$ term and the corresponding flux rates were simply interpreted as transfers between \mathbf{b} fields of different Fourier modes using $\mathbf{j} = \nabla \times \mathbf{b}$. However, recent studies showed that a clear phenomenological picture can be obtained if we decompose the $\nabla \times (\mathbf{u} \times \mathbf{b})$ term in ordinary MHD as $-(\mathbf{u} \cdot \nabla) \mathbf{b}$ and $(\mathbf{b} \cdot \nabla) \mathbf{u}$ [31,32]. For the sake of uniformity with MHD nonlinearities and to get further physical insights, it is thus reasonable to decompose the Hall contribution in the induction equation in a similar way. Such a decomposition results in two contributions $-d_i \mathbf{b} \cdot (\mathbf{b} \cdot \nabla) \mathbf{j}$ and $d_i \mathbf{b} \cdot (\mathbf{j} \cdot \nabla) \mathbf{b}$ in the magnetic energy evolution equation $(\mathbf{b} \cdot \partial_t \mathbf{b})$ representing \mathbf{j} -to- \mathbf{b} and \mathbf{b} -to- \mathbf{b} transfer, respectively.

In this paper, using 3D direct numerical simulation of 256^3 spatial resolution, we present a systematic study comparing the individual contribution of the aforementioned subparts of the Hall term in the small-scale dynamo action. For the sake of computational convenience, here we have calculated the fluxes using mode-to-mode (M2M) transfers [31,33]. Such a methodology is particularly useful in the study of dynamos as it helps in classifying different types of energy transfers depending on the length scales (or equivalently the wave vectors). To recognize the Hall contribution unambiguously, we have employed a ∇^4 hyperviscosity. Similar to the previous studies, a clear signature of backscatter of magnetic energy due to the Hall term is also observed. Of all possible contributions, the transfer from small-scale \mathbf{j} fields to large scale [34] \mathbf{b} fields is found to be the most efficient one. Furthermore, the maximum of the total transfer rate to large-scale \mathbf{b} fields shifts towards larger scales as we go on increasing d_i .

The rest of the paper is organized as follows: In Sec. II, we describe the basic equations of incompressible HMHD and expressions for spectral fluxes using M2M formalism. Section III A contains the description of the code and details of the numerical simulations. In Secs. III B and III C, we present different contributions to magnetic energy transfer to large-scale \mathbf{b} fields and their variation with d_i , respectively. Finally, in Sec. IV, we discuss our findings and conclude.

II. MODE-TO-MODE ENERGY TRANSFERS AND SPECTRAL FLUXES

We start with the incompressible Hall MHD equations [5]

$$\partial_t \mathbf{u} - \nu \nabla^2 \mathbf{u} = -(\mathbf{u} \cdot \nabla) \mathbf{u} + (\mathbf{b} \cdot \nabla) \mathbf{b} - \nabla \left(p + \frac{b^2}{2} \right) + \mathbf{f}, \quad (2)$$

$$\partial_t \mathbf{b} - \eta \nabla^2 \mathbf{b} = -(\mathbf{u} \cdot \nabla) \mathbf{b} + (\mathbf{b} \cdot \nabla) \mathbf{u} + d_i (\mathbf{j} \cdot \nabla) \mathbf{b} - d_i (\mathbf{b} \cdot \nabla) \mathbf{j}, \quad (3)$$

$$\nabla \cdot \mathbf{u} = 0, \quad \nabla \cdot \mathbf{b} = 0, \quad (4)$$

where p is the kinetic pressure (normalized by the constant fluid density ρ), \mathbf{f} is the external force per unit mass, ν and η denote the kinematic viscosity and the magnetic diffusivity, respectively. As mentioned in the Introduction, the last two terms on the right-hand side of Eq. (3) correspond to the Hall effect. The total energy E ($= \int (u^2 + b^2)/2 d\tau$) is an inviscid invariant of both incompressible MHD and HMHD [23,24,35].

To investigate the detailed conservation of energy, one requires the evolution equations for modal energy densities $E_{\mathbf{k}}^u$ ($= \mathbf{u}_{\mathbf{k}} \cdot \mathbf{u}_{\mathbf{k}}^*/2$) and $E_{\mathbf{k}}^b$ ($= \mathbf{b}_{\mathbf{k}} \cdot \mathbf{b}_{\mathbf{k}}^*/2$). First, we calculate the Fourier transforms of Eqs. (2) and (3) and then the corresponding complex conjugates. Finally, using straightforward algebra, for the inertial zone, one can show

$$\partial_t E_{\mathbf{k}}^u = \frac{1}{2} \int_{\mathbf{p}} \int_{\mathbf{q}} [S_E^{uu}(\mathbf{k}|\mathbf{p}, \mathbf{q}) + S_E^{ub}(\mathbf{k}|\mathbf{p}, \mathbf{q})] \delta(\mathbf{k} + \mathbf{p} + \mathbf{q}) d\mathbf{p} d\mathbf{q}, \quad (5)$$

$$\partial_t E_{\mathbf{k}}^b = \frac{1}{2} \int_{\mathbf{p}} \int_{\mathbf{q}} [S_E^{bb}(\mathbf{k}|\mathbf{p}, \mathbf{q}) + S_E^{bu}(\mathbf{k}|\mathbf{p}, \mathbf{q}) + d_i S_E^{\mathcal{H}}(\mathbf{k}|\mathbf{p}, \mathbf{q})] \delta(\mathbf{k} + \mathbf{p} + \mathbf{q}) d\mathbf{p} d\mathbf{q}, \quad (6)$$

where $S_E^{xy}(\mathbf{k}|\mathbf{p}, \mathbf{q})$ is the generic form of combined transfer rate of energy from $\mathbf{y}_{\mathbf{p}}$ and $\mathbf{y}_{\mathbf{q}}$ to $\mathbf{x}_{\mathbf{k}}$ and can be mathematically expressed as

$$|S_E^{xy}(\mathbf{k}|\mathbf{p}, \mathbf{q})| = \Im[(\mathbf{p} \cdot \mathbf{z}_{\mathbf{q}})(\mathbf{y}_{\mathbf{p}} \cdot \mathbf{x}_{\mathbf{k}}) + (\mathbf{q} \cdot \mathbf{z}_{\mathbf{p}})(\mathbf{y}_{\mathbf{q}} \cdot \mathbf{x}_{\mathbf{k}})], \quad (7)$$

where \mathbf{x} , \mathbf{y} , and \mathbf{z} can be \mathbf{u} and \mathbf{b} , and \Im denotes the coefficient of the imaginary part of a complex number. The algebraic sign becomes negative only when \mathbf{x} and \mathbf{y} represent the same field. Note that the \mathbf{z} fields neither donate nor receive any energy in the process but only act as a mediator. $S_E^{\mathcal{H}}(\mathbf{k}|\mathbf{p}, \mathbf{q})$ is the combined magnetic energy transfer rate due to the Hall term only and can be mathematically expressed as

$$S_E^{\mathcal{H}}(\mathbf{k}|\mathbf{p}, \mathbf{q}) = \Im[(\mathbf{p} \cdot \mathbf{b}_{\mathbf{q}})(\mathbf{j}_{\mathbf{p}} \cdot \mathbf{b}_{\mathbf{k}}) + (\mathbf{q} \cdot \mathbf{b}_{\mathbf{p}})(\mathbf{j}_{\mathbf{q}} \cdot \mathbf{b}_{\mathbf{k}}) - (\mathbf{p} \cdot \mathbf{j}_{\mathbf{q}})(\mathbf{b}_{\mathbf{p}} \cdot \mathbf{b}_{\mathbf{k}}) - (\mathbf{q} \cdot \mathbf{j}_{\mathbf{p}})(\mathbf{b}_{\mathbf{q}} \cdot \mathbf{b}_{\mathbf{k}})]. \quad (8)$$

For ordinary MHD as well as HMHD, $S_E^{uu}(\mathbf{k}|\mathbf{p}, \mathbf{q})$ and $S_E^{bb}(\mathbf{k}|\mathbf{p}, \mathbf{q})$ individually satisfy triadic conservations whereas $S_E^{ub}(\mathbf{k}|\mathbf{p}, \mathbf{q})$ and $S_E^{bu}(\mathbf{k}|\mathbf{p}, \mathbf{q})$ together follow a conservation in each triad. Using Eq. (8), one can also obtain

$$S_E^{\mathcal{H}}(\mathbf{k}|\mathbf{p}, \mathbf{q}) + S_E^{\mathcal{H}}(\mathbf{p}|\mathbf{q}, \mathbf{k}) + S_E^{\mathcal{H}}(\mathbf{q}|\mathbf{k}, \mathbf{p}) = 0, \quad (9)$$

where $S_E^{\mathcal{H}}(\mathbf{p}|\mathbf{q}, \mathbf{k})$ and $S_E^{\mathcal{H}}(\mathbf{q}|\mathbf{k}, \mathbf{p})$ are obtained under the cyclic permutation of the wave vectors. Thus, the detailed conservation of total energy in HMHD can be written as

$$\partial_t (E_{\mathbf{k}}^u + E_{\mathbf{k}}^b + E_{\mathbf{p}}^u + E_{\mathbf{p}}^b + E_{\mathbf{q}}^u + E_{\mathbf{q}}^b) = 0.$$

According to Kraichnan, the triads constitute the fundamental unit of energy transfer in the Fourier space [36,37]. However, some previous studies further decomposed the combined transfer rate as a sum of two M2M transfer rates as in the following manner:

$$S_E^{xy}(\mathbf{k}|\mathbf{p}, \mathbf{q}) = T_E(\mathbf{y}_{\mathbf{p}} \xrightarrow{\mathbf{z}_{\mathbf{q}}} \mathbf{x}_{\mathbf{k}}) + T_E(\mathbf{y}_{\mathbf{q}} \xrightarrow{\mathbf{z}_{\mathbf{p}}} \mathbf{x}_{\mathbf{k}}), \quad (10)$$

where $T_E(\mathbf{y}_{\mathbf{p}} \xrightarrow{\mathbf{z}_{\mathbf{q}}} \mathbf{x}_{\mathbf{k}})$ is interpreted as the M2M transfer rate of energy from the giver field $\mathbf{y}_{\mathbf{p}}$ to the receiver field $\mathbf{x}_{\mathbf{k}}$ with $\mathbf{z}_{\mathbf{q}}$ acting as a mediator [31–33,38]. Note that the M2M transfer rates are always defined up to an additive arbitrary constant [32,38]. However, the calculation of flux and

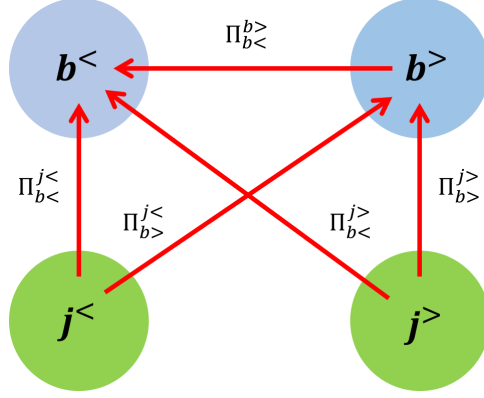


FIG. 1. Schematic diagram of various magnetic energy fluxes due to the Hall term.

shell-to-shell transfer rates are not affected by such constants which cancel out in individual triads. As mentioned before, in this paper, the Hall term is decomposed in two parts and the combined energy transfer rate corresponding to the \mathbf{k} th mode is given by

$$S_E^{\mathcal{H}}(\mathbf{k}|\mathbf{p}, \mathbf{q}) = \Sigma_E^{bj}(\mathbf{k}|\mathbf{p}, \mathbf{q}) + \Sigma_E^{bb}(\mathbf{k}|\mathbf{p}, \mathbf{q}), \quad (11)$$

where

$$\Sigma_E^{bj}(\mathbf{k}|\mathbf{p}, \mathbf{q}) = \Im[(\mathbf{p} \cdot \mathbf{b}_q)(\mathbf{j}_p \cdot \mathbf{b}_k) + (\mathbf{q} \cdot \mathbf{b}_p)(\mathbf{j}_q \cdot \mathbf{b}_k)] \quad \text{and} \quad (12)$$

$$\Sigma_E^{bb}(\mathbf{k}|\mathbf{p}, \mathbf{q}) = -\Im[(\mathbf{p} \cdot \mathbf{j}_q)(\mathbf{b}_p \cdot \mathbf{b}_k) + (\mathbf{q} \cdot \mathbf{j}_p)(\mathbf{b}_q \cdot \mathbf{b}_k)] \quad (13)$$

represent the \mathbf{j} -to- \mathbf{b} and \mathbf{b} -to- \mathbf{b} transfers, respectively. In analogy with the ordinary MHD case, here one can immediately understand that Σ_E^{bj} and Σ_E^{bb} originate from the terms $-(\mathbf{b} \cdot \nabla)\mathbf{j}$ and $(\mathbf{j} \cdot \nabla)\mathbf{b}$, respectively. From Eq. (13), one can immediately derive

$$\Sigma_E^{bb}(\mathbf{k}|\mathbf{p}, \mathbf{q}) + \Sigma_E^{bb}(\mathbf{p}|\mathbf{q}, \mathbf{k}) + \Sigma_E^{bb}(\mathbf{q}|\mathbf{k}, \mathbf{p}) = 0, \quad (14)$$

and combining Eqs. (9) and (14) one can finally obtain

$$\Sigma_E^{bj}(\mathbf{k}|\mathbf{p}, \mathbf{q}) + \Sigma_E^{bj}(\mathbf{p}|\mathbf{q}, \mathbf{k}) + \Sigma_E^{bj}(\mathbf{q}|\mathbf{k}, \mathbf{p}) = 0. \quad (15)$$

In this paper, we are interested in the contribution of the Hall term in the dynamo action. We are therefore only concerned with the feeding of large-scale magnetic fields and hence we numerically calculate the fluxes $\Pi_{b<}^{b>}$, $\Pi_{b<}^{j<}$, and $\Pi_{b<}^{j>}$, and their mathematical expressions are given by

$$\Pi_{b<}^{b>}(k_0) = -d_i \sum_{|\mathbf{k}| \leq k_0} \sum_{|\mathbf{p}| > k_0} \Im[(\mathbf{p} \cdot \mathbf{j}_q)(\mathbf{b}_p \cdot \mathbf{b}_k)], \quad (16)$$

$$\Pi_{b<}^{j<}(k_0) = d_i \sum_{|\mathbf{k}| \leq k_0} \sum_{|\mathbf{p}| \leq k_0} \Im[(\mathbf{p} \cdot \mathbf{b}_q)(\mathbf{j}_p \cdot \mathbf{b}_k)], \quad (17)$$

$$\Pi_{b<}^{j>}(k_0) = d_i \sum_{|\mathbf{k}| \leq k_0} \sum_{|\mathbf{p}| > k_0} \Im[(\mathbf{p} \cdot \mathbf{b}_q)(\mathbf{j}_p \cdot \mathbf{b}_k)], \quad (18)$$

where $\Pi_{x>}^{y<}(k_0)$ is the net energy transfer rate from all modes inside the sphere of radius k_0 of field y to all modes outside k_0 of field x [see Fig. 1]. Finally, the total flux to the large-scale \mathbf{b} field can simply be calculated using

$$\Pi_{b<} = \Pi_{b<}^{b>} + \Pi_{b<}^{j<} + \Pi_{b<}^{j>}. \quad (19)$$

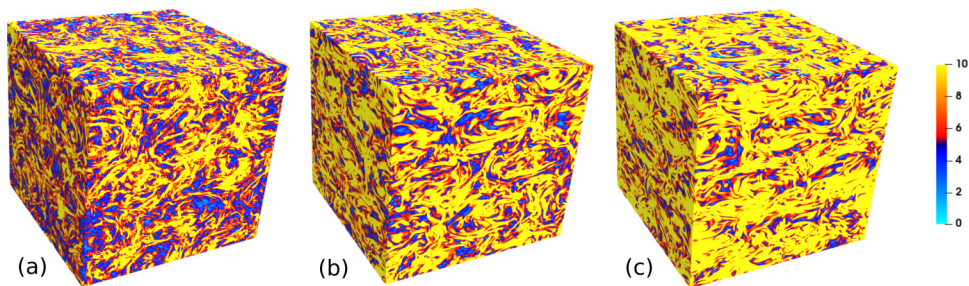


FIG. 2. Absolute values of current densities for (a) $d_i = 0.2$, (b) $d_i = 0.1$, and (c) $d_i = 0.05$ at $t = 45$.

III. NUMERICAL RESULTS

A. Methodology

Here we perform a three-dimensional direct numerical simulation of Eqs. (2)–(4) for $d_i = 0.05$, 0.1, and 0.2. The simulations are performed using a parallel pseudospectral code based on the parallelization scheme by Mortensen and Langtangen [39]. The box length is taken to be 2π and periodic boundary conditions have been assumed in all three spatial directions. To remove the aliasing error, the 2/3-dealiasing rule has been used so the maximum available wave number $k_{\max} \approx 85$ [40]. The equations are evolved using a fourth-order Runge-Kutta (RK4) method with a fixed time step $dt (= 5 \times 10^{-4})$. The flow is forced with a nonhelical $(\nabla \times \mathbf{f} \perp \mathbf{f})$ Taylor-Green (TG) forcing $\mathbf{f} = (\sin(k_0 x)\cos(k_0 y)\cos(k_0 z), -\cos(k_0 x)\sin(k_0 y)\cos(k_0 z), 0)$ with $k_0 = 2$. For the sake of finding a clear Hall contribution, here we implement fourth-order hyperdissipative operators for dissipation. Following a general prescription of dynamo simulation, initially a pure hydrodynamic run (with hyperviscosity) was made to reach a turbulent steady state. After that, a random seed magnetic field was introduced at small scales ($k > 10$) such that the initial ratio of magnetic to kinetic energy was $\sim 10^{-3}$. Finally, the full HMHD equations were solved until the magnetic energy reaches saturation. Note that the magnetic Prandtl number (P_m) for our simulations is kept at unity.

In Fig. 2, we display snapshots of absolute values of current densities for three different ion inertial lengths. As one can expect, the current density contours tend to flatten out with increasing d_i [from right to left in Fig. 2] due to dissipative effects. The left panel of Fig. 3 shows the time

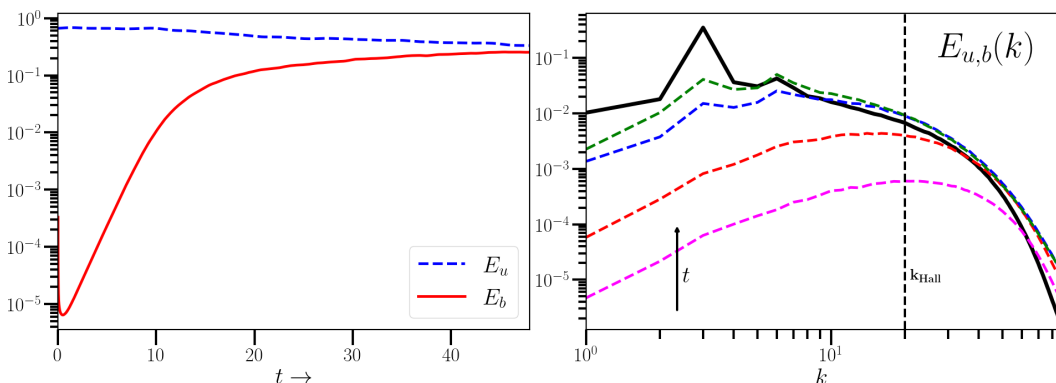


FIG. 3. Left panel: Total kinetic energy (blue dashed curve) and total magnetic energy (red solid curve) versus time. Right panel: Power spectra for magnetic energy for various times (dashed curves). The black solid curve corresponds to power spectra for kinetic energy at $t = 45$. The ion inertial length d_i is taken to be 0.05, which corresponds to $k_{\text{Hall}} = 20$ (denoted by the vertical dashed line).

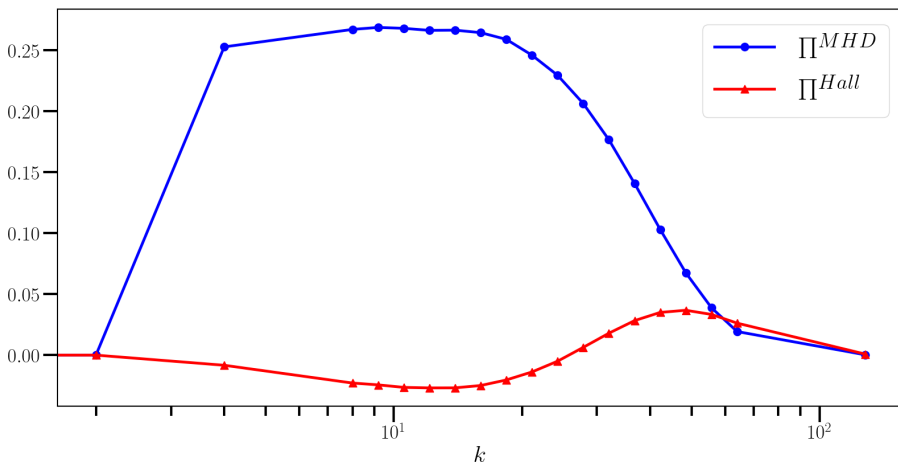


FIG. 4. Total MHD versus Hall flux rates for $d_i = 0.05$ at $t = 45$.

evolution of kinetic and magnetic energies whereas the right panel shows their spectral distributions. After an initial transient period, the magnetic energy grows exponentially. In this regime, the magnetic fields are approximately frozen in the bulk flow and hence the corresponding dynamo can be characterized as a kinematic-MHD dynamo. As time progresses, the electron flow starts to get decoupled from the bulk and another regime of kinematic-HMHD dynamos is reached where the magnetic field lines are effectively frozen in the electron fluid. Finally, the magnetic field saturates where it becomes strong enough to affect the motion of the flow, thus leading to a nonkinematic HMHD dynamo. From the spectral distribution, it is easy to verify that large-scale ($k < 10$) magnetic fields grow with time. However, the large-scale magnetic field grows much faster than small-scale magnetic fields, which effectively saturates near $t = 20$. Both of these observations are consistent with previous results on dynamo simulations in HMHD [26,30].

B. Spectral fluxes

To get an estimate between the MHD and Hall transfers, we first plot the total flux rates. For our calculations, we have chosen the following radii: 2.00, 4.00, 8.00, 9.19, 10.56, 12.12, 13.93, 16.00, 18.40, 21.11, 24.25, 27.86, 32.00, 36.75, 42.22, 48.50, 55.71, 64.00, and 128.00. Such a logarithmic choice of radii is adopted to populate the inertial range where a power law scaling is expected to hold [41].

Figure 4 shows the total transfer rates for magnetic energy, calculated using the M2M formalism described before. The Hall term contains a higher order derivative as compared to MHD nonlinear terms and is of the same order as ordinary dissipation terms ($\sim \nabla^2$). Therefore, the hyperviscous operators ($\sim \nabla^4$) are simply used to exclusively capture the Hall contribution free from ordinary viscous effects. Note that the total Hall flux obtained in our current paper is approximately increased by two times than those obtained in the previous studies where ordinary viscosities were used [26,30]. However, comparing the Hall fluxes in aforementioned papers and the current paper (see Fig. 4), one can immediately see that the hyperviscosity does not alter the global nature of the Hall flux. As mentioned before, a clear backscatter of magnetic energy due to the Hall effect is observed for wave numbers smaller than $k_{Hall} (\approx 20)$. To further probe the aforesaid backscatter, we compute scale-classified fluxes using Eqs. (16)–(18).

Figure 5 shows the flux rates corresponding to all possible channels responsible for the feeding of the large-scale magnetic field for three different times $t = 10, 20,$ and 45 . Such choices of time steps have been made to elucidate the role of Hall effect at the kinematic-MHD dynamo regime, Hall saturated nonlinear dynamos, and, finally, at the stage of magnetic energy saturation, respectively.

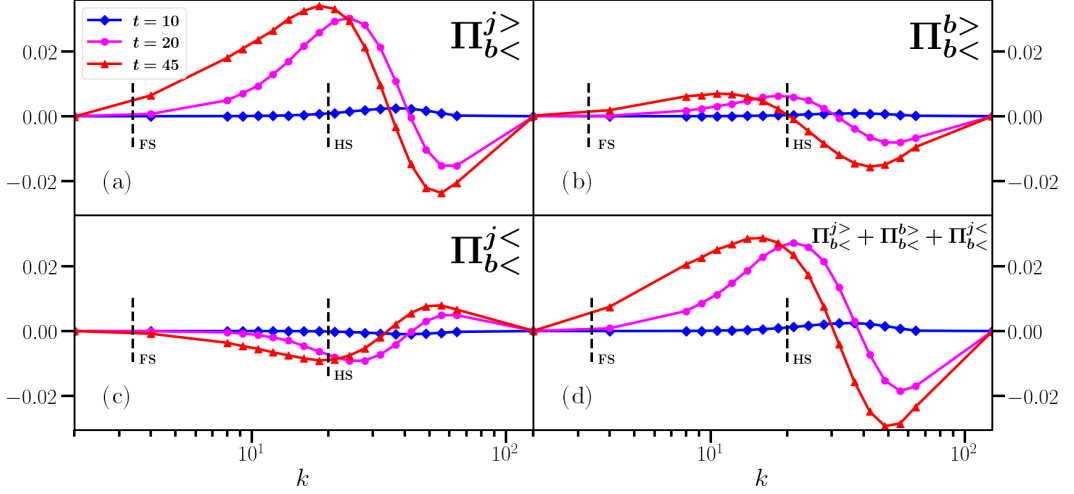


FIG. 5. Various scale-to-scale fluxes important for dynamos at different times. FS = forcing scale, HS = Hall scale.

Figure 5(a) shows the variation of $\Pi_{b<}^{j>}$ with k . A positive flux rate directly represents the net transfer of magnetic energy from the small-scale \mathbf{j} field to large-scale \mathbf{b} field (dynamo action) and vice versa. At $t = 10$, the flux rate is slightly positive beyond the Hall scale (k_{Hall}). As time progresses, the transfer rate becomes larger. Interestingly, the flux rate is not sign definite and, in fact, it changes signs for length scales superior to the Hall scale. At $t = 20$, the flux changes signs around $k = 40$ whereas for $t = 45$ the sign change occurs around $k = 30$. Hence, with time, the transition wave number is found to shift towards the Hall scale ($k = 20$). For $t = 45$, where the magnetic energy saturates (see Fig. 3), the maximum of the positive flux rate peaks around the Hall scale. Figure 5(b) shows the variation of $\Pi_{b<}^{b>}$ with wave numbers. A positive flux rate therefore signifies a net transfer of magnetic energy from small- to large-scale \mathbf{b} field. Similar to $\Pi_{b<}^{j>}$, at $t = 10$, the transfer rate is found to be slightly positive beyond the Hall scale. At $t = 20$, the flux rate increases and becomes negative beyond $k = 40$. Note that a negative flux rate in this case signifies a transfer towards the small-scale \mathbf{b} field, i.e., a direct cascade. For $t = 45$, the positive peak of the flux rate is found to shift further towards smaller wave numbers while the change of sign occurs around Hall scale ($k = 20$). Figure 5(c) shows the variation of $\Pi_{b<}^{j<}$ with k . It denotes the transfer of magnetic energy from the large-scale \mathbf{j} field to large-scale \mathbf{b} field. At $t = 10$, in contrast to the previous cases, the flux rate is found to be slightly negative beyond the Hall scale. A negative flux rate signifies that the large-scale magnetic field loses energy instead of gaining. Thus, in the kinematic regime, the large-scale current fields remove energy from the large-scale magnetic fields rather than feeding them. As time progresses, both positive and negative flux rates increase. At $t = 20$, it changes signs from negative to positive around $k = 45$ whereas at $t = 45$ the sign change takes place around $k = 30$. In addition, the peak of negative flux rate is also found to move towards the Hall scale. Of all the aforementioned transfer rates, clearly $\Pi_{b<}^{j>}$ is the largest. It signifies that the small-scale \mathbf{j} fields are the primary contributor in sustaining large-scale \mathbf{b} fields. Similarly, $\Pi_{b<}^{b>}$ also contributes in dynamo action through the transfer of magnetic energy from small-scale \mathbf{b} fields to large-scale \mathbf{b} fields. However, $\Pi_{b<}^{j<}$ does not directly seem to enhance the large-scale magnetic fields, rather it facilitates the growth of small-scale magnetic fields. The sum of all aforesaid transfers is the net transfer rate of magnetic energy to large scales. Therefore, a positive value denotes that a dynamo action can be maintained through the scale-to-scale transfer from various scales. Figure 5(d) shows the variation of total flux rate $\Pi_{b<}^{j>} + \Pi_{b<}^{b>} + \Pi_{b<}^{j<}$ with k . Interestingly, it shows similar behavior to

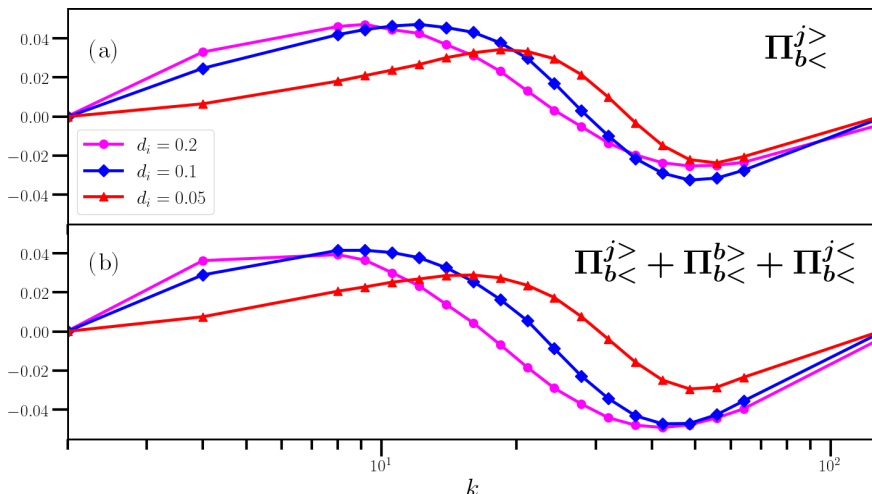


FIG. 6. (a) $\Pi_{b<}^{j>}$ and (b) $\Pi_{b<}^{j>} + \Pi_{b<}^{b>} + \Pi_{b<}^{j<}$ versus d_i at $t = 45$.

that of $\Pi_{b<}^{j>}$. This is expected since out of all three individual fluxes, $\Pi_{b<}^{j>}$ is the most dominating one.

C. Dependence of transfer rates on Hall scale

In this section, we study the variation of aforementioned flux rates with d_i . We have performed three simulations with $d_i = 0.05, 0.1,$ and 0.2 with the corresponding Hall wave numbers given by 20, 10, and 5 respectively. Note that, for our simulations, the forcing wave number $k_f \approx 3.4$. Instead of studying the variation of fluxes with d_i for different times, here we only consider their values at magnetic energy saturation ($t = 45$). Figure 6(a) shows the variation of $\Pi_{b<}^{j>}$ with k for different values of d_i . As d_i is increased, the Hall wave number decreases i.e., the Hall contribution becomes effective for lower k values. Correspondingly, the peak value of the flux rates also shift towards smaller wave numbers with increasing d_i . In addition, the wave numbers where the fluxes change signs also moves to lower values. In accordance with the findings in the previous section, $\Pi_{b<}^{j>}$ fluxes are found to be the strongest irrespective of the value of the d_i . The other two fluxes, although weaker than $\Pi_{b<}^{j>}$, shows similar behavior with the change in d_i (not shown here). Figure 6(b) shows the total flux rates to the large-scale \mathbf{b} field for different Hall parameters. As expected, the total flux rates also mimic the nature of the most dominating contribution $\Pi_{b<}^{j>}$.

IV. DISCUSSION AND CONCLUSIONS

In this paper, we have systematically investigated the spectral space energy transfer due to the Hall effect in three-dimensional HMHD turbulence. In particular, we have studied the role of the Hall term on the growth of a large-scale magnetic field, i.e., the dynamo effect. Extending the previous studies, where a clear backscatter of magnetic energy was observed, here we have further probed into the said backscatter using spectral fluxes. Unlike the previous studies, here the Hall term has been decomposed into two parts, $-d_i(\mathbf{b} \cdot \nabla)\mathbf{j}$ and $d_i(\mathbf{j} \cdot \nabla)\mathbf{b}$. The current study clearly shows that the first term, representing the \mathbf{j} - \mathbf{b} interaction, contributes primarily to the dynamo action. Further classification of the transfer rates in scale-specific subparts $\Pi_{b<}^{j>}$, $\Pi_{b<}^{b>}$, and $\Pi_{b<}^{j<}$ shows that the large-scale \mathbf{b} field is mainly fed by the small-scale \mathbf{j} field (Fig. 5). In particular, near the Hall scale, the maximum energy transfer takes place from small-scale \mathbf{j} to large-scale \mathbf{b} field, whereas the large-scale \mathbf{j} field extracts energy from the large-scale \mathbf{b} field. However, the net effect mimics

the nature of $\Pi_{b<}^{j>}$ which is the strongest of the three aforesaid transfers. All the flux rates change signs at some wave number which moves towards the Hall scale with time. This further verifies the dual cascading nature of the Hall effect found in previous studies [26,30]. Finally, the sum all three contributions clearly shows that the Hall term adds a non-negligible contribution to the small-scale dynamo action. Finally, the global nature of the flux transfer does not change with the change in the ion inertial length d_i .

A thorough understanding of different channels of energy transfer in HMHD is extremely useful to quantify the contribution of the Hall term in sub-MHD scale turbulence in space plasmas, e.g., the solar wind, the magnetospheric plasmas, etc. Furthermore, the Hall effect can be extremely important in explaining the generation of large-scale magnetic fields in several astrophysical bodies through the dynamo effect. In addition, during both the kinematic and the saturated regime, the Hall effect is known to introduce nonlocality in the scale-to-scale energy transfer process. More specifically, it has been shown that the magnetic energy shows local forward and nonlocal inverse cascade. The net effect of these two aforesaid processes give rise to previously mentioned backscatter of magnetic energy for wave numbers smaller than the Hall scale [26,30]. Therefore, it would be interesting to study how the individual parts contribute to the nonlocality. Our study can also be extended to various other plasma systems such as compressible plasmas, electron-MHD, extended-MHD, etc. More specifically, the nonlinear terms present in the aforementioned systems can be decomposed in a similar manner to the Hall term and their individual contributions can be studied in the scale-to-scale transfer process using numerical simulations and *in situ* observational data.

ACKNOWLEDGMENTS

The authors thank F. Plunian and N. Pan for useful discussions. The simulation code is developed by the first author with the help of parallelization schemes given in Ref. [39]. The simulations are performed using the support and resources provided by PARAM Sanganak under the National Supercomputing Mission, Government of India at the Indian Institute of Technology, Kanpur. M.K.S. acknowledges Tarang for cross-referencing the code for flux calculation [42]. S.B. acknowledges DST-INSPIRE faculty Research Grant No. DST/PHY/2017514 and CEFIPRA Research Grant No. 6104-01.

-
- [1] U. Frisch and A. Kolmogorov, *Turbulence: The Legacy of A. N. Kolmogorov* (Cambridge University Press, Cambridge, UK, 1995).
 - [2] S. B. Pope, *Turbulent Flows* (IOP Publishing, Bristol, UK, 2001), Vol. 12, pp. 2020–2021.
 - [3] H. Tennekes and J. L. Lumley, *A First Course in Turbulence* (MIT Press, Massachusetts, USA, 1972).
 - [4] D. Biskamp, *Magnetohydrodynamic Turbulence* (Cambridge University Press, Cambridge, UK, 2003).
 - [5] S. Galtier, *Introduction to Modern Magnetohydrodynamics* (Cambridge University Press, Cambridge, UK, 2016).
 - [6] J. Bittencourt, *Fundamentals of Plasma Physics* (Springer, New York, 2013).
 - [7] G. Belmont, R. Grappin, F. Mottez, F. Pantellini, and G. Pelletier, *Collisionless Plasmas in Astrophysics* (Wiley, New York, USA, 2013).
 - [8] N. Andrés, S. Galtier, and F. Sahraoui, Exact law for homogeneous compressible Hall magnetohydrodynamics turbulence, *Phys. Rev. E* **97**, 013204 (2018).
 - [9] E. Papini, L. Franci, S. Landi, A. Verdini, L. Matteini, and P. Hellinger, Can Hall magnetohydrodynamics explain plasma turbulence at sub-ion scales? *Astrophys. J.* **870**, 52 (2019).
 - [10] S. Galtier, von Kármán-Howarth equations for Hall magnetohydrodynamic flows, *Phys. Rev. E* **77**, 015302(R) (2008).

- [11] S. Banerjee and S. Galtier, Chiral exact relations for helicities in Hall magnetohydrodynamic turbulence, *Phys. Rev. E* **93**, 033120 (2016).
- [12] R. Meyrand and S. Galtier, Spontaneous Chiral Symmetry Breaking of Hall Magnetohydrodynamic Turbulence, *Phys. Rev. Lett.* **109**, 194501 (2012).
- [13] S. Galtier, On the origin of the energy dissipation anomaly in (Hall) magnetohydrodynamics, *J. Phys. A: Math. Theor.* **51**, 205501 (2018).
- [14] S. Galtier, Wave turbulence in incompressible Hall magnetohydrodynamics, *J. Plasma Phys.* **72**, 721 (2006).
- [15] R. Ferrand, S. Galtier, F. Sahraoui, R. Meyrand, N. Andrés, and S. Banerjee, On exact laws in incompressible Hall magnetohydrodynamic turbulence, *Astrophys. J.* **881**, 50 (2019).
- [16] S. Galtier and E. Buchlin, Multiscale Hall-magnetohydrodynamic turbulence in the solar wind, *Astrophys. J.* **656**, 560 (2007).
- [17] P. Hellinger, A. Verdini, S. Landi, L. Franci, and L. Matteini, von Kármán-Howarth equation for Hall magnetohydrodynamics: Hybrid simulations, *Astrophys. J.* **857**, L19 (2018).
- [18] N. Andrés, F. Sahraoui, S. Galtier, L. Z. Hadid, R. Ferrand, and S. Y. Huang, Energy Cascade Rate Measured in a Collisionless Space Plasma with MMS Data and Compressible Hall Magnetohydrodynamic Turbulence Theory, *Phys. Rev. Lett.* **123**, 245101 (2019).
- [19] R. Bandyopadhyay, L. Sorriso-Valvo, A. Chasapis, P. Hellinger, W. H. Matthaeus, A. Verdini, S. Landi, L. Franci, L. Matteini, B. L. Giles *et al.*, *In Situ* Observation of Hall Magnetohydrodynamic Cascade in Space Plasma, *Phys. Rev. Lett.* **124**, 225101 (2020).
- [20] A. Choudhuri, *The Physics of Fluids and Plasmas: An Introduction for Astrophysicists* (Cambridge University Press, Cambridge, UK, 1998).
- [21] A. Brandenburg, D. Sokoloff, and K. Subramanian, Current status of turbulent dynamo theory: From large-scale to small-scale dynamos, *Space Sci. Rev.* **169**, 123 (2012).
- [22] F. Rincon, Dynamo theories, *J. Plasma Phys.* **85**, 205850401 (2019).
- [23] P. D. Mininni, D. O. Gomez, and S. M. Mahajan, Dynamo action in magnetohydrodynamics and Hall-magnetohydrodynamics, *Astrophys. J.* **587**, 472 (2003).
- [24] P. D. Mininni, D. O. Gomez, and S. M. Mahajan, Direct simulations of helical Hall-MHD turbulence and dynamo action, *Astrophys. J.* **619**, 1019 (2005).
- [25] P. Mininni, A. Alexakis, and A. Pouquet, Shell-to-shell energy transfer in magnetohydrodynamics. II. Kinematic dynamo, *Phys. Rev. E* **72**, 046302 (2005).
- [26] P. D. Mininni, A. Alexakis, and A. Pouquet, Energy transfer in Hall-MHD turbulence: Cascades, backscatter, and dynamo action, *J. Plasma Phys.* **73**, 377 (2007).
- [27] M. Lingam and A. Bhattacharjee, Hall current effects in mean-field dynamo theory, *Astrophys. J.* **829**, 51 (2016).
- [28] R. Kumar, M. K. Verma, and R. Samtaney, Energy transfers and magnetic energy growth in small-scale dynamo, *Europhys. Lett.* **104**, 54001 (2013).
- [29] Z. Yoshida and S. M. Mahajan, Variational Principles and Self-Organization in Two-Fluid Plasmas, *Phys. Rev. Lett.* **88**, 095001 (2002).
- [30] D. O. Gómez, P. D. Mininni, and P. Dmitruk, Hall-magnetohydrodynamic small-scale dynamos, *Phys. Rev. E* **82**, 036406 (2010).
- [31] M. K. Verma, Statistical theory of magnetohydrodynamic turbulence: Recent results, *Phys. Rep.* **401**, 229 (2004).
- [32] F. Plunian, R. Stepanov, and M. K. Verma, On uniqueness of transfer rates in magnetohydrodynamic turbulence, *J. Plasma Phys.* **85**, 905850507 (2019).
- [33] G. Dar, M. K. Verma, and V. Eswaran, Energy transfer in two-dimensional magnetohydrodynamic turbulence: Formalism and numerical results, *Physica D* **157**, 207 (2001).
- [34] The large scale field here signifies the magnetic field between the forcing and the seed field scale.
- [35] S. Servidio, W. H. Matthaeus, and V. Carbone, Ergodicity of ideal Galerkin three-dimensional magnetohydrodynamics and Hall magnetohydrodynamics models, *Phys. Rev. E* **78**, 046302 (2008).
- [36] R. H. Kraichnan, Irreversible statistical mechanics of incompressible hydromagnetic turbulence, *Phys. Rev.* **111**, 1747 (1958).

- [37] R. H. Kraichnan, The structure of isotropic turbulence at very high Reynolds numbers, *J. Fluid Mech.* **5**, 497 (1959).
- [38] G. Dar, Energy spectra and transfers in magnetohydrodynamic turbulence, Ph.D. thesis, Indian Institute of Technology Kanpur, India, 2000.
- [39] M. Mortensen and H. P. Langtangen, High performance python for direct numerical simulations of turbulent flows, *Comput. Phys. Commun.* **203**, 53 (2016).
- [40] S. A. Orszag, On the elimination of aliasing in finite-difference schemes by filtering high-wavenumber components, *J. Atmos. Sci.* **28**, 1074 (1971).
- [41] R. Kumar and M. K. Verma, Amplification of large-scale magnetic field in nonhelical magnetohydrodynamics, *Phys. Plasmas* **24**, 092301 (2017).
- [42] M. K. Verma, A. Chatterjee, K. S. Reddy, R. K. Yadav, S. Paul, M. Chandra, and R. Samtaney, Benchmarking and scaling studies of pseudospectral code Tarang for turbulence simulations, *Pramana* **81**, 617 (2013).